Journal of Neuroscience Research 68:681–690 (2002)

Role of Long-Range Repulsive Forces in Organizing Axonal Neurofilament Distributions: Evidence From Mice Deficient in Myelin-Associated Glycoprotein

Sanjay Kumar,[1] Xinghua Yin,[2] Bruce D. Trapp,[2] Michael E. Paulaitis,[3] and Jan H. Hoh[1,3]*

[1]Department of Physiology, Johns Hopkins University School of Medicine, Baltimore, Maryland
[2]Department of Neurosciences, Lerner Research Institute, Cleveland Clinic Foundation, Cleveland, Ohio
[3]Department of Chemical Engineering, Johns Hopkins University, Baltimore, Maryland

When the axon of a motor neuron is sectioned and visualized by electron microscopy, a two-dimensional distribution of neurofilaments (NFs) with nonrandom spacing is revealed; this ordered arrangement implies the presence of physical interactions between the NFs. To gain insight into the molecular basis of this organization, we characterized NF distributions from mouse sciatic nerve cross sections using two statistical mechanical measures: radial distribution functions and occupancy probability distributions. Our analysis shows that NF organization may be described in terms of effective pairwise interactions. In addition, we show that these statistical mechanical measures can detect differences in NF architecture between wild-type and myelin-associated glycoprotein null mutant mice. These differences are age dependent, with marked contrast between the NF distributions by 9 months of age. Finally, using Monte Carlo simulations, we compare the experimental results with predictions for models in which adjacent NFs interact through rigid cross bridges, deformable cross bridges, and long-range repulsive forces. Among the models tested, a model in which the filaments interact through a long-range repulsive force is most consistent with the results of our analysis.

Key words: cytoskeleton; intermediate filaments; unstructured proteins; phosphorylation; interaction forces; amyotrophic lateral sclerosis

Neurofilaments (NFs) are the most abundant cytoskeletal element of large, myelinated axons. These type IV intermediate filaments have contour lengths of several micrometers and run in parallel along the axon. When the axon is cut in cross section and the transected NFs are visualized by electron microscopy (EM), the NF distribution appears nonrandomly arranged, suggesting that the filaments interact with one another to maintain order. One metric for this order is the distribution of nearest-neighbor spacings, which typically reveals that most nearest-neighbor separation distances fall within a relatively narrow range (e.g., 33–47 nm for adult rats; Hsieh et al., 1994). Experimental nearest-neighbor spacings have also been compared with simulated distributions of highly ordered and randomly positioned particles; based on this study, it was concluded that NF distributions lie intermediate between completely random and highly ordered (Hsieh et al., 1994). Other approaches have been used to characterize structure in NF distributions, including the use of tile-counting methods (Price et al., 1988, 1993).

Much attention has been paid to the biochemistry of interfilament interactions. NFs are composed of three polypeptide subunits: a light chain (NF-L; 61 kD in humans), a medium chain (NF-M; 90 kD), and a heavy chain (NF-H; 110 kD). The amino termini of the monomers contain rod domains, which associate to form the filament backbone, and the carboxy termini of NF-M and -H form "sidearms" that protrude from the filament backbone to give the isolated NF a bottle-brush appearance (Geisler and Weber, 1981; Willard and Simon, 1981; Hisanaga and Hirokawa, 1988; Leapman et al., 1997). The sidearms, which are heavily phosphorylated (Lee et al., 1988), are thought to mediate interactions between NFs and allow them to form a structural framework that maintains axonal patency and protects the bore of the axon from compressive stress (Brown and Hoh, 1997; Gou et al., 1998). There are several hypotheses for the nature of these interactions. One proposed mechanism is electrostatic repulsion between the phosphorylated sidearms; this is supported by several observations, including a correlation between regional NF phosphorylation level and interfilament spacing distance (Carden et al., 1987; de Waegh et

*Correspondence to: Jan H. Hoh, Department of Physiology, Johns Hopkins University School of Medicine, 725 N. Wolfe Street, Baltilmore, MD 21205. E-mail: jhoh@jhmi.edu

Received 17 December 2001; Accepted 4 March 2002

al., 1992). A second model is interfilament cross bridging mediated by the sidearms, which is based primarily on the observation of connecting structures between NF backbones by EM (Chen et al., 2000) and rheological measurements (Leterrier et al., 1996). In a third model, the sidearms lack a stable three-dimensional structure and move rapidly to occupy a large effective volume, giving rise to an entropic repulsion upon compression. This model is supported by atomic force microscopy (AFM) measurements, which demonstrate molecular exclusion in the proximity of NFs; independent experiments have detected a long-range repulsive force between individual NFs and the AFM probe even in high-salt buffer (Brown and Hoh, 1997). Consistent with this finding, Dunker and colleagues screened the Swiss-Prot database with a neural network predictor trained to identify long disordered regions of proteins and found that the mouse NF-H sidearm domain received the sixth-highest score among more than 59,000 total sequences (Romero et al., 1998).

Anterograde axonal transport of NFs is also the subject of much controversy, with some groups favoring a model in which fully assembled NF polymers are transported along the axon and others favoring one in which individual NF subunits or short oligomers are transported and then added into existing mature filaments (Terada et al., 1996; Galbraith et al., 1999; Brown, 2000). Moreover, there is disagreement among proponents of the former model regarding whether NFs are transported as single filaments or as bundles (Wang et al., 2000; Yabe et al., 2001). Understanding the physical nature of NF–NF interactions in the axon bears obvious implications for each of these models.

To understand better the relationship between interfilament interaction mechanisms and observed interfilament spacing in vivo, we have applied statistical mechanical methods to analyze NF distributions from sciatic nerve cross sections. To determine the utility of this approach for studying phenotypic changes in interfilament interactions, we have compared NF distributions from wild-type mice with those from myelin-associated glycoprotein (MAG) –/– mice. MAG is a heavily glycosylated type I integral membrane protein that is enriched in the myelin internode membrane that apposes the axon. The MAG –/– phenotype was chosen as a comparison because it has been characterized extensively and includes marked reductions in nearest-neighbor NF spacing, mean axonal diameter, and NF phosphate content. MAG directly or indirectly serves, based on these findings, as an axonal ligand that influences the phosphorylation state of NFs, which, in turn, regulates interfilament spacing and axonal diameter (Yin et al., 1998). To explore which models of interfilament interaction might account for the results of the analysis, we performed Monte Carlo (MC) simulations of two-dimensional NF distributions in which we imposed interfilament potentials designed to model different sidearm interactions.

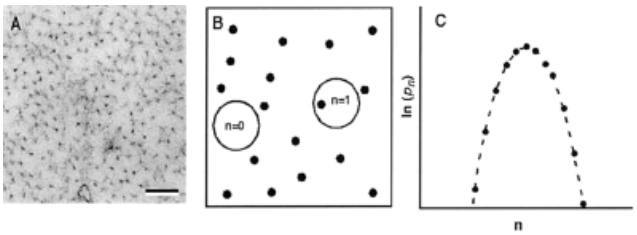

Fig. 1. Schematic diagram of information theory approach. **A:** Electron microscopy of a motor neuron axon cut in cross section; the punctate structures are NFs. **B:** Schematic representation (at higher magnification) of NFs and observation circles. Observation circles of a fixed diameter are placed in the field, and the numbers of NFs observed in the circle (n) are recorded. **C:** Occupancy numbers are converted into a probability distribution (p_n) by constructing a histogram and normalizing by the number of observations. The dashed line represents a Gaussian fit, which appears parabolic on these semilogarithmic axes. Scale bar = 100 nm.

MATERIALS AND METHODS

Theory

The potential of mean force (PMF) provides a means of connecting interaction potentials between particles with their arrangement in space. One recently developed approach to connecting the PMF to the structural arrangement of particles involves the application of information theory (IT; Hummer et al., 1996). The central quantity in this approach is the occupancy probability distribution, defined in the context of NF organization as the distribution of probabilities p_n of finding n NFs in an axon cross-sectional area of defined size and shape. To calculate the occupancy probability distribution for an ensemble of axon cross sections, we place a spherical observation "area" at a large number of random positions within the cross section (Fig. 1A) and count the number of NFs that fall within each area (Fig. 1B). A normalized histogram is then constructed to yield the distribution of probabilities of finding a given number of NFs in the observation area (Fig. 1C). The moments of this distribution are directly related to the cross-sectional density and radial distribution function of NFs in the ensemble of axon cross sections. The PMF is directly related to the radial distribution function.

The p_n distribution shown in Figure 1C is analyzed be defining an information entropy (η) in terms of p_n:

$$\eta = -\sum_{n=0}^{N} p_n \ln(p_n/\hat{p}_n).$$

Here, the set $\hat{p}_n$ is a set of prior distributions, which we chose to be unbiased (constant $\hat{p}_n$ for $n = 0 \ldots N$), and N is large compared with the average of n. The most likely p_n distribution is obtained by maximizing η under constraints of the available information, i.e., that satisfy conditions imposed by the moments of the distribution. In particular, for the zeroth moment,

$$\langle n^0 \rangle = \sum p_n = 1,$$

and, for the first moment,

$$\langle n^1 \rangle = \sum np_n = \rho \Delta A,$$

where ρ is the number density of NFs in cross section and ΔA is the observation area, and, for the second moment,

$$\langle n^2 \rangle = \sum n^2 p_n = \langle n \rangle + \rho^2 \int_{\Delta A} dr \int_{\Delta A} g|(r-r')|\, dr.$$

Here $g(r)$ is the radial distribution function characterizing spatial correlations between pairs of NFs and, as such, is related to the PMF through the expression PMF $= -kT\ln[g(r)]$. Radial distribution functions have been used to quantify structure and interaction potentials between connexins in gap junctions (Braun et al., 1984, 1987) and immunoglobulin receptors (Perelson, 1978) and bacteriorhodopsin proteins in membrane arrays (Pearson et al., 1983). The statistical descriptors obtained from IT have been used successfully to relate intermolecular structure and intermolecular interactions in water (Hummer et al., 1996) and polymeric fluids (Garde et al., 2000). Maximizing η subject to the three moment constraints leads to a Gaussian distribution for p_n, which has several implications. Most significantly, a Gaussian probability distribution indicates that the organization of the system may be described in terms of pair correlations alone, i.e., the PMF calculated directly from the radial distribution function. Descriptions of higher order correlations among three or more NFs are not required. The first moment or mean of this Gaussian distribution corresponds to the NF number density in cross section, and the variance, which is related to the second moment, provides a measure of the interfilament PMF or, equivalently, the strength of interfilament interactions. For a given density, the smaller the variance about the mean, the stronger the pair correlations between NFs.

Analysis of Electron Micrographs

Electron micrographs were obtained from wild-type and MAG −/− mice at ages 14 days, 3 months, and 9 months. The procedures for perfusion and fixation of tissue as well as microscopy have been described elsewhere (Yin et al., 1998). Micrographs were then scanned and digitized (6–12 EMs for each cohort); a region containing 200–1,000 NFs and relatively free of organelles and other cytoskeletal structures was chosen, and the coordinates of each NF within the region were identified by hand and recorded. These coordinates were used to calculate radial distribution functions and probability curves. Computer code for this analysis and for the MC simulations described below were written in Fortran. Gaussian fits for both experimental and simulation results were performed as quadratic fits to $\ln(p_n)$ which adds statistical weight to the extremes of the distribution.

MC Simulations

NF cross sections were represented as two-dimensional disks in canonical ensemble MC simulations carried out at 300K (Allen and Tildseley, 1987). An initial configuration was generated by placing the disks at the nodes of a square lattice. Metropolis MC moves were made one randomly chosen particle at a time until the system reached equilibrium, as determined by a constant average total energy and radial distribution function. After equilibration, the simulation run was continued to obtain the occupancy probability distributions, which were calculated as averages over 30–50 structures sampled at fixed intervals (approximately every 10–15 MC cycles).

Interactions between the disks were modeled using an analytical potential function representing pair interactions between polymer brushes. Specifically, we used a potential function based on an expression for gelatin-coated hard spheres (Likos et al., 2000). This spherical interaction potential is taken to be a reasonable approximation for the interaction potential between pairs of parallel cylinders, as would be the case for NFs aligned in the axon. To our knowledge, the latter potential function is not available. In this model, the NF–NF interaction potential, $U(r)$, is a function of center-to-center separation distance between NF cylinders or disks in cross section. The NF sidearms will occupy a diffuse volume that extends a distance, L, from the filament backbone, which has radius R_c. The NF backbones are not allowed to overlap, so that $U(r) = \infty$ for $r < 2R_c$. When the NFs are sufficiently far apart that the sidearm layers do not overlap (i.e., $r > 2R_c + 2L$), the NFs do not interact and $U(r) = 0$. At intermediate distances, the potential is given by:

$$U(\gamma) = kT\alpha \frac{16\pi R_c L^2}{35 s^3} \times \alpha \left[28(\gamma^{-1/4} - 1) + \frac{20}{11}(1 - \gamma^{11/4}) + 12(\gamma - 1) \right],$$

where $\gamma = (r - 2R_c)/(2L)$. Here, kT is the thermal energy, s is the distance between sidearms along the NF backbone, and α is a scaling factor empirically determined to be 0.01. Based on estimates from EM of isolated NFs (Geisler and Weber, 1981), we took $R_c = 5$ nm and $s = 3$ nm. We used a square-well potential to represent rigid cross bridging and a soft repulsive potential of the above-described form superimposed on a square-well potential to represent deformable cross bridging.

RESULTS

We first determined the occupancy probability distributions and radial distribution functions for wild-type and MAG −/− mice at 9 months of age (Fig. 2). The radial distribution function has a direct structural interpretation and can provide insights not apparent in the probability distributions. This being the case, direct calculations of radial distribution functions complement their more indirect representation in the IT approach. The occupancy probability curves for wild-type and MAG −/− are Gaussian (Fig. 2A), consistent with the IT prediction for a system whose organization is governed by a collection of pairwise interactions. Insight into the physical properties of the two NF architectures may be obtained by comparing the statistical descriptors of the two distributions. The means of the wild-type and MAG −/− distributions are

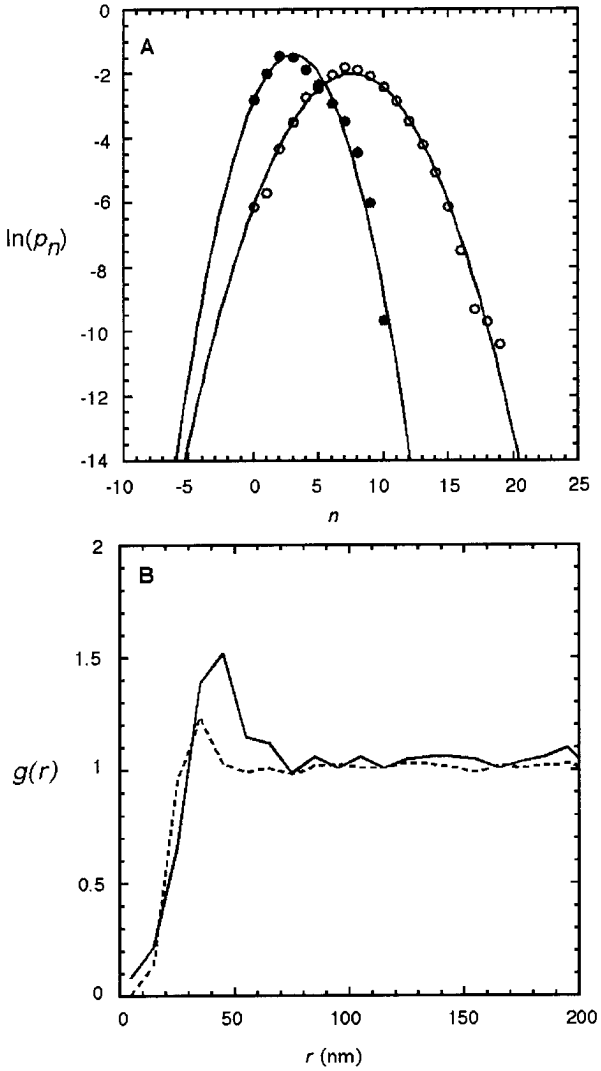

Fig. 2. **A:** Experimental probability distributions at 9 months. Points are experimental values for wild-type mice (solid circles) and MAG −/− mice (open circles) using an observation circle radius of 60 nm, with Gaussian fits. **B:** Experimental radial distribution functions at 9 months. Wild type is represented by a solid line and MAG −/− by a dashed line.

approximately 2.6 and 7.4, respectively, reflecting the fact that the NFs are more densely packed in the axons of the MAG −/− animals than in those of the wild type. In addition, the standard deviations of the curves differ substantially at approximately 1.7 for the wild-type group and 2.5 for the MAG −/− group (a fractional difference of 0.47 times the wild-type value). Within the IT framework, this difference demonstrates weaker pair correlations and greater disorder in the MAG −/− NF distributions. This, in turn, suggests that interfilament interaction forces are weaker in the MAG −/− mice than in wild-type mice. This is seen more readily through direct measurement of the radial distribution functions (Fig. 2B). The wild-type NFs show greater interfilament spacing as evidenced by

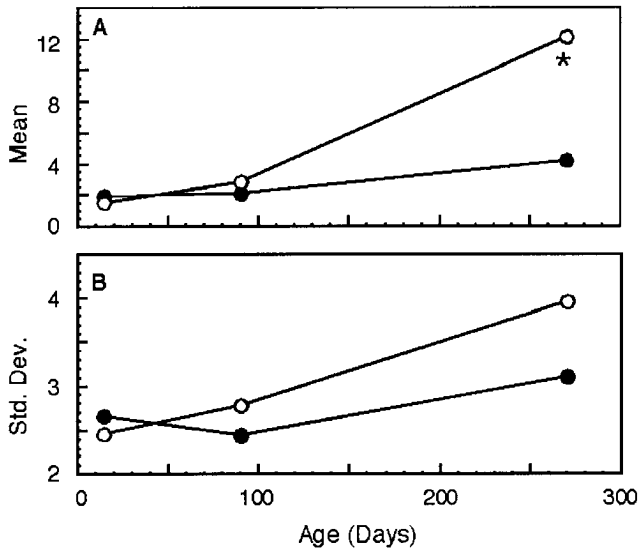

Fig. 3. Mean (**A**) and standard deviation (**B**) of wild-type (solid circles) and MAG −/− (open circles) probability distributions over time. $\star P < 0.01$ by Student's *t*-test. Note that here we used an 80-nm-radius window (rather than 60 nm as for Fig. 2) for all ages to obtain more meaningful p_n statistics for the smaller NF densities of the 14-day-old mice. This change in window size has no qualitative effect on the results.

the right-shifted peak; they also show greater structure on this length scale as evidenced by a higher first peak value in *g(r)*.

The IT approach was further tested by examining changes in NF distributions during development (Fig. 3). We performed IT analysis on axonal cross sections from wild-type and MAG −/− at ages 14 days and 3 months, in addition to the 9-month-old mice described above. In this analysis, the densities of the two populations track one another closely through 3 months but diverge significantly by 9 months (Fig. 3A). Similar developmental changes are observed in the width of the probability distributions (Fig. 3B).

An attractive feature of the statistical mechanical approach described here is that it provides measurable quantities (p_n and *g(r)*) that change with interaction potentials. To determine whether proposed models of interfilament interaction are capable of accounting for the trends observed in the experimental data (Fig. 2), we conducted MC simulations on two-dimensional arrays of particles representing NF cross sections. In these simulations, we fixed the density, volume, and temperature of the system, imposed a pairwise interaction potential representing a physical model, and assessed the resulting configurations using IT and radial distribution functions. We tested three models: a rigid cross-bridging model (Chen et al., 2000), a soft cross-bridging model, and an entropic repulsion model (Brown and Hoh, 1997). In each case, we simulated two NF densities, one corresponding to the NF density of the wild-type mice at 9 months and the other

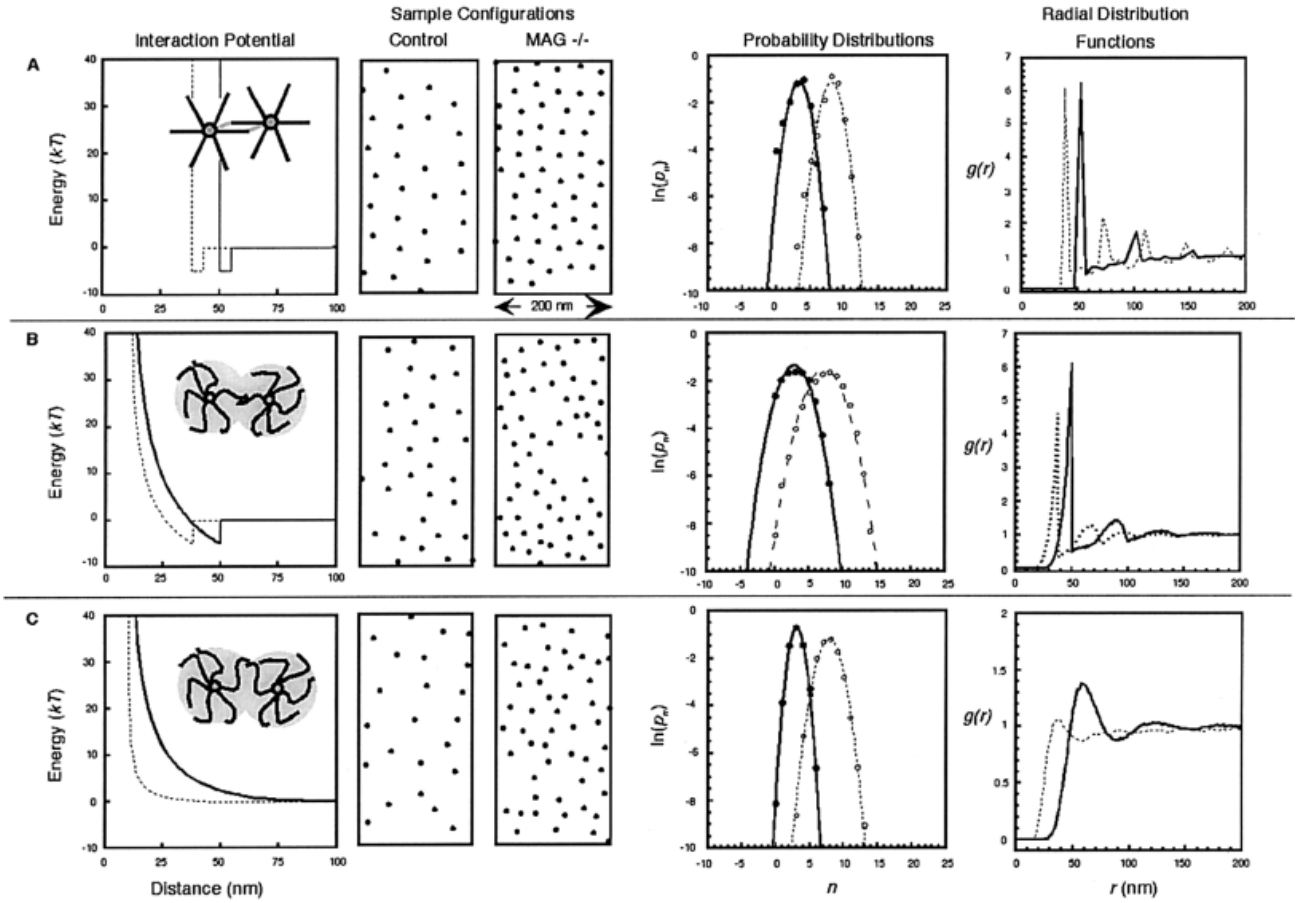

Fig. 4. Monte Carlo simulations for three model NF interaction potentials: rigid cross-bridging model (**A**), soft cross-bridging model (**B**), and entropic repulsion model (**C**). The leftmost panels depict the potentials used in the simulation to represent the wild-type and MAG −/− NFs along with a schematic physical model (**insets**). Note that the width of the potential well in A is exaggerated for clarity. The next two panels show examples of configurations sampled during a typical simulation for each case. The next panel depicts the resulting probability distributions for the simulation with Gaussian fits, and the rightmost panel depicts radial distribution functions for each case (note scales). Solid lines and solid circles represent wild-type and dashed lines and open circles represent MAG −/− mice.

corresponding to that of the MAG −/− mice. We did not attempt to model a purely electrostatic spacing mechanism, because doing so requires the three-dimensional charge distribution (i.e., shape of the protein), which is not known. This is because under physiological ionic conditions the Debye screening length is approximately 0.5 nm, and direct electrostatic interactions are negligible on the length scale of interfilament spacings.

We first considered the cross-bridging or "rigid strut" model (Fig. 4A), in which the NF architecture results from a sidearm of one filament binding rigidly to the backbone or sidearm of an adjacent filament. We assume that there is a narrow region of binding sites along the NF sidearm, with a modest binding energy of $5kT$. The corresponding interaction potential is a narrow energy well placed at a fixed interfilament distance. We assume that the sidearms may not penetrate one another, so that at separation distances less than the strut position an infinitely steep potential is encountered. At distances greater than the strut position, the interaction potential is zero; inside the well, the NFs bind. Simulations were run at interfilament binding distances corresponding to approximate average nearest-neighbor distances in wild-type and MAG −/− mice (~38 and 50 nm, respectively) and at the appropriate respective densities (Fig. 4A). Inspection of typical configurations for each case indicates that, under this potential, the NFs are regularly spaced, with some voids that result from interfilament adhesion and clustering. The probability distributions deviate slightly from Gaussian predictions, particularly at low n; similar results have been observed in other attractive (self-associating) systems. At 1.08 and 1.10 for wild-type and MAG −/−, respectively (fractional difference of 0.019 times the wild-type value), the standard deviations of the two probability distributions are similar, unlike the case for the experimental data (Fig. 2). The radial distribution functions also differ substantially from the experimental data; the hard repulsion gives rise to a step-like increase in $g(r)$ at the strut

position and the adhesive well produces sharp, periodic spikes. When the adhesive well is reduced or removed entirely, the probability distributions more tightly follow Gaussian fits, and the spikes broaden and fall in amplitude (not shown).

To test the sensitivity of the cross-bridging simulation result to well depth (binding energy), well position (interfilament binding distance), and well width (binding range), we ran several simulations in which each of these parameters was systematically varied. These simulations produced results similar to those shown in Figure 4; we were unable to find, within a reasonable parameter space, conditions that qualitatively recapitulated the experimental results of Figure 2. We also tested potentials in which the sidearms were allowed to penetrate one another without binding, i.e., where the narrow adhesive well was retained at the position shown but the hard wall separation distance was reduced to 10 nm (the NF core diameter). These simulations produced aphysical configurations in which the cross bridge between a pair of NFs overlapped the core of a third NF (not shown), leading us to reject such potentials as inaccurate descriptions of the physical model. More sophisticated potentials that incorporate correlations of three or more NFs were also rejected because the experimental probability distributions indicate that the NF architecture arises from pairwise additive interactions.

Next, we considered a model in which the NFs interact via soft or deformable cross bridges (the "soft strut" model; Fig. 4B). Here, as in the rigid strut model, the NFs do not interact beyond separation distances corresponding to the strut position; inside the strut position, the NFs bind with energy $5kT$. However, the NFs are now allowed to approach one another more closely than the binding distance, where they remain bound but encounter an increasingly repulsive potential with closer approach. This soft repulsion represents the deformation of the cross bridge, which could result from bending of a folded protein or compression of an unfolded protein. To simulate this model, we retained the cross bridge positions of the rigid strut model, used a soft repulsive component to represent the wild-type potential, and used a shorter range, soft repulsive component for the MAG −/− potential (Fig. 4B). As expected, sample configurations now reveal some NF pairs separated by distances less than the strut position. However, the attractive component still produces moderate NF clustering. Because of this, the probability distributions again deviate slightly from Gaussian predictions; the fit improves when either the repulsive component is strengthened or the attractive component is weakened (not shown). The standard deviations of the probability distributions, which were1.7 for wild-type and 1.9 for MAG −/− (a fractional difference of 0.12 times the wild-type value), do not differ as greatly as in the experimental results. The distributions are broader than those produced by the rigid strut potentials because of the greater diversity of interfilament spacings made possible by the soft repulsion. The periodic maxima in the radial distribution functions now develop gradually, a consequence of the soft repulsion; however, the spikes that are not seen in the experimental data persist.

Finally, we considered the entropic repulsion model (Fig. 4C). Here, the NFs interact through a long-range (>50 nm) repulsive force generated by the thermally driven motion of the unstructured sidearms. To represent this model analytically, we used a potential based on the Alexander-DeGennes expression for polypeptide-coated hard spheres. The key physical parameter here is the effective thickness of the unstructured polypeptide layer (the "brush"); by varying this parameter in our simulation, we found that at each density, as the layer thickness is increased, the variance of the probability curve falls (not shown). This reflects the stronger interfilament interactions at greater brush thicknesses. To determine whether this model could account for the experimental data, we ran simulations at the wild-type NF density with a brush thickness of 50 nm and the MAG −/− NF density with a thickness of 25 nm, estimates for highly and poorly extended sidearms (Fig. 4C). Inspection of sample configurations for each case indicates that the presence of extended sidearms is capable of generating much long-range order at low (wild-type) NF density. This is further evident in the probability distributions, which show differences in the standard deviation of the distribution for MAG −/− and wild-type that are similar to those in the experiment (0.82 for wild-type and 1.3 for MAG −/−, a fractional difference of 0.59 times the wild-type value). The radial distribution functions show broad maxima consistent with a soft repulsive potential. The wild-type maximum is both greater in magnitude and right shifted relative to the MAG −/− maximum. Moreover, the curves are notable for the absence of the sharp spikes observed in the cross-bridging model. We also performed simulations in which the brush thickness was fixed but the NF density was varied; we were unable to reproduce the experimental result at the densities of interest.

DISCUSSION

The central finding that emerges from the probability distribution analysis is that axonal NF distributions may be described in terms of pairwise additive NF–NF interactions. This is evidenced by the observation that experimental occupancy probability distributions are Gaussian. A second finding is that this analysis can detect phenotypic alterations in NF distributions associated with genetic ablation of MAG. These differences are age dependent, with phenotypic differences most prominent at 9 months. This parallels the observed developmental course of mean axonal caliber and nerve degeneration in MAG −/− mice (Yin et al., 1998). Interpreting the parameters of these distributions using IT, we find that NF distributions from MAG −/− mice are more densely packed yet show weaker interfilament correlations. Those differences suggest weaker pair interactions in the MAG −/− axons, an interpretation supported by experimental determination of the radial distribution function. The finding that axonal NF distributions may be represented in terms of pair interactions bears at least two important consequences.

First, it enables us to conduct MC simulations in which pair interaction potentials are used, which, in turn, allows us to test the effect of interfilament repulsion and attraction on the overall structure of NF distributions and to determine which interaction potentials best account for the phenotypic changes observed in the absence of MAG. Second, it implies that the correct physical model is one in which only the relative positions of two NFs have to be known to determine the potential energy. This excludes more complex models in which the interaction potential between two NFs depends on the position of a third.

Based on these findings, we conducted MC simulations to test three models of NF–NF interactions: rigid interfilament cross bridging, soft (flexible) interfilament cross bridging, and entropic repulsion mediated by disordered sidearms. The results of the simulations show that the presence of a long-range repulsive interfilament potential between the NF sidearms best accounts for the experimentally observed NF architectures in vivo. The probability distributions calculated for a rigid cross-bridging model do not agree well with the experimental data. Furthermore, the radial distribution functions for this model have sharp spikes that are absent in the experimental data. Using a mixed potential to represent a soft cross bridge improves agreement of the simulations and data with respect to the radial distribution functions. However, the spikes that are not seen in the experimental data persist in the simulations; moreover, in both cases, the attractive component of the potential favors NF aggregation, which, in turn, produces deviations from Gaussian behavior. The purely repulsive long-range potential captures the changes in probability distributions when the magnitude of the repulsion is decreased in the MAG −/− mice.

Interfilament cross bridging is widely regarded as an important regulator of interfilament spacing, based largely on the observation of such structures by EM (Hisanaga and Hirokawa, 1988; Chen et al., 2000). It is therefore somewhat surprising that a purely repulsive model of NF–NF interactions accounts for the phenotypic changes observed in the absence of MAG. One candidate cross-bridging protein is the neuronal isoform of bullous pemphigoid antigen 1 (BPAG1-n), whose gene locus encodes a rich variety of splice variants, which cross-link several cytoskeletal proteins (Leung et al., 2001). Recently, BPAG1-n was reported to cross-link microtubules (MTs) and bind and coalign NFs to the actin cytoskeleton in transfected cells (Yang et al., 1996, 1999). However, in a subsequent report from another group, the ability of BPAG1-n to bind several NF fragments was examined using fluorescence colocalization, three-hybrid analysis, and in vitro binding assays (Leung et al., 1999). These investigators found that the NF triplet bound BPAG1-n only when the sidearm of NF-H was genetically ablated. The authors hypothesized, based on these findings, that the sidearm domain blocked or otherwise interfered with binding. Similarly, NF-H and NF-M were found not to bind themselves or one another in a yeast two-hybrid screen unless the tails were removed (Leung and Liem, 1996). Both results are consistent with the model presented here, in which the disordered sidearm domains sterically exclude binding partners. Additional data appearing to support the cross-bridging model are that transgenic mice with low axonal NF densities show clustered NFs with nearest-neighbor spacings similar to those in wild-type (Xu et al., 1996). However, these transgenic strains also have greatly increased numbers of axonal MTs (to the point, in fact, where the microtubules completely dominate the axonal cytoskeleton). Little is known about NF–MT interactions; if those interactions are highly repulsive, or if MT–MT interactions are highly attractive, then one would observe separation of the MTs and NFs into distinct phases. Indeed, BPAG1-n has recently been shown to bind and organize neuronal MTs (Yang et al., 1999). Phase separation of this type is routinely observed in synthetic polymer mixtures (Bates, 1991). Finally, there are several examples of cases in which decreases in NF density are accompanied by increases in interfilament spacing (de Waegh et al., 1992; Nixon et al., 1994; Yin et al., 1998; Martin et al., 1999). Taken together with the possibility of compensatory changes, support for the cross-bridging model by the transgenic animal studies is equivocal. A repulsive interfilament potential is also most consistent with the experimental finding that, when the axonal membrane is chemically disrupted, the NFs diffuse apart freely (Brown and Lasek, 1993).

It should also be noted that our findings do not imply that attractive interfilament interactions never exist, merely that they do not appear to play a dominant role in organizing NF distributions in the system characterized here. Moreover, the depiction of the sidearms as unstructured is not mutually exclusive with attractive interactions between the sidearms. Disordered polymers may attract one another through mutual entanglement (Doi and Edwards, 1986) or through specific chemical interactions (Zilman and Safran, 2001). These interactions have been addressed analytically only recently. They are expected to assume a more complex analytical form than the binding potentials used here; superimposition of these interactions onto repulsive potentials may in fact yield simulation results that are more easily reconciled with the experimental data.

Our analysis suggests that the observed MAG −/− phenotype is the result of weaker interfilament repulsion despite higher NF density. Thus, one question that arises is the mechanism by which the strength of this repulsion might be modulated. There are several candidates for the origin of this modulation, including changes in sidearm phosphorylation and O-GlcNAc modification. Analysis of the murine NF-H sidearm sequence indicates that, although it is extremely rich in charged residues (285 of 679 residues), these residues are nearly evenly divided between cationic and anionic (147 D and E, 138 R and K); the balance is even tighter in human NF-H (155 D and E, 154 R and K). The NF-H sidearm is normally very heavily phosphorylated; for example, squid giant axon NF-H has been shown to contain more than 100 phosphates per sidearm, representing near-maximal phosphorylation of

consensus kinase targets. The phosphorylated NF sidearms have a significant net negative charge and from a polymer perspective can be viewed as a polyelectrolyte. Unstructured polyelectrolyte brushes have been well studied (Lodge and Muthukumar, 1996; Luckham, 1996; Szleifer and Carignano, 1996; Tirrell and Levicky, 1997; Zhao and Brittain, 2000). In particular it has been shown that the size (thickness) of the brush is directly dependent on the net charge of the polymer (Pincus, 1991). Increasing the charge increases intramolecular monomer repulsion, which, in turn, effectively swells the brush resulting in a longer range repulsion. In the case of NFs from MAG –/– axons, it has been shown by immunoblotting of whole nerve homogenates and immunogold staining of axonal cross sections that NF-M and NF-H sidearm phosphorylation is markedly reduced relative to wild type (Yin et al., 1998). In the polymer view, this change in phosphorylation represents a modulation in polymer charge, which would reduce the predicted repulsive potential. This reduction in repulsive potential is in agreement with the experimental and simulation results presented here and suggests a mechanism for regulating interfilament spacing (Fig. 5). Here, NFs in wild-type mice are abundantly phosphorylated and interact via a long-range entropic exclusion mechanism; absent MAG, this phosphorylation is reduced, the sidearms are consequently less extended, and the interactions are more short range. This interpretation is further supported by in vitro studies that reveal that dephosphorylation alters both sidearm hydrodynamic radius (Chin et al., 1989) and NF gel viscoelastic properties (Gou et al., 1998). We note that we are not the first to propose a model in which sidearm phosphorylation produces increased interfilament spacing through increased phosphate–phosphate repulsion; for example, de Waegh et al. (1992) invoked such a model to explain a correlation between regional phosphorylation level and interfilament spacing. We agree with these investigators that electrostatic repulsion plays a fundamental role, but our results suggest that this role is far more short ranged. Rather than directly mediating interactions between NFs, we propose that electrostatic repulsion governs structure within each NF, which, in turn, gives rise to long-range repulsion.

There is also considerable evidence that phosphorylation is an important physiologic regulator of interfilament spacing. One example of this is the finding that sidearm phosphorylation is often heavy in the distal axon, where parallel NF distributions are found, and relatively light in the cell body, where NFs form a more clustered network (Nixon et al., 1994). Electron energy loss spectroscopy studies in squid giant axon have demonstrated a reciprocal relationship between NF density and phosphorylation; as NF density falls distally to the cell body, phosphorylation and axonal caliber rise (Martin et al., 1999). A recent study found coexisting populations of differentially phosphorylated NFs with dramatically different transport and morphological properties (Yabe et al., 2001); another study found regional variations in phosphorylation along single filaments (Brown, 1998). Both further support

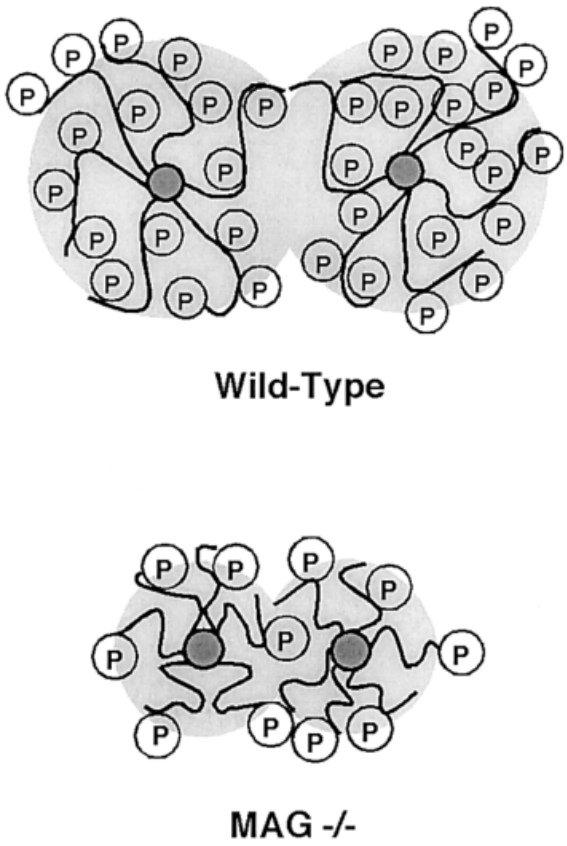

Fig. 5. Proposed biochemical mechanism for modulating interfilament spacing. Wild-type NF sidearms are extensively phosphorylated and negatively charged, producing expanded unstructured sidearms and long-range repulsion. Conversely, MAG –/– NFs are less phosphorylated, leading to weaker intrachain repulsion between monomers and a sidearm that is collapsed relative to the wild type. This in turn leads to a shorter range interfilament repulsion.

phosphorylation as a spatially localized regulator of NF architecture. In an entropic repulsion model, the highly phosphorylated sidearms produce an expanded sidearm layer that leads to mutual steric exclusion and the maintenance of interfilament spacing. Dephosphorylation reduces steric exclusion, thereby exposing potential binding sites or facilitating the formation of nonaligned NF networks.

The entropic repulsion model also bears implications for the issue of anterograde NF transport. A primarily repulsive model of NF–NF interaction would allow for transportation of individual filaments along the axon. Indeed, transport of individual NF polymers has been directly visualized in several recent fluorescence studies, one of which suggested that >97% of axonal NFs move as single filaments (Wang et al., 2000; Wang and Brown, 2001). The observation that NFs are transported individually is less compatible with a model in which NFs are highly cross-linked. Additional recent studies suggest that axonal NFs exist in highly diverse states, moving as bun-

dles under some conditions and individually under others (Yabe et al., 2001).

We have used radial distribution functions and occupancy probability distributions to analyze axonal distributions of NFs and characterize phenotypic differences between wild-type and MAG −/− mice. We show that NF distributions are governed by pair correlations, that wild-type and MAG −/− mice have distinct probability distributions, and that differences between the two are best explained by a model in which the NFs interact through a repulsive potential that weakens in MAG −/− mice. We propose that these differences in potentials are due to changes in phosphorylation. The analytical framework presented here offers a way to quantify order in NF distributions and directly relate that order to interfilament potentials. This approach may prove useful in detecting subtle changes in NF architecture in animal models of neurodegenerative disease, studying interfilament interactions in vitro, and ultimately relating intermolecular organization to interaction forces for a variety of biological macromolecules.

ACKNOWLEDGMENTS

This work was supported by grants from the National Institutes of Health (Medical Scientist Training Program Fellowship to S.K., grant NS38186 to B.D.T.), the U.S. Army (grant DAMD 17-99-1-9488 to J.H.H.), and the National Science Foundation (grant CTS-0078491 to M.E.P.).

REFERENCES

Allen MP, Tildseley DJ. 1987. Computer simulation of liquids. Oxford: Oxford Science Publications.

Bates FS. 1991. Polymer–polymer phase behavior. Science 251:898–905.

Braun J, Abney JR, Owicki JC. 1984. How a gap junction maintains its structure. Nature 310:316–318.

Braun J, Abney JR, Owicki JC. 1987. Lateral interactions among membrane-proteins—valid estimates based on freeze-fracture electron-microscopy. Biophys J 52:427–439.

Brown A. 1998. Contiguous phosphorylated and non-phosphorylated domains along axonal neurofilaments. J Cell Sci 111:455–467.

Brown A. 2000. Slow axonal transport: stop and go traffic in the axon. Nat Rev Mol Cell Biol 1:153–156.

Brown A, Lasek RJ. 1993. Neurofilaments move apart freely when released from the circumferential constraint of the axonal plasma membrane. Cell Motil Cytoskel 26:313–324.

Brown HG, Hoh JH. 1997. Entropic exclusion by neurofilament sidearms: a mechanism for maintaining interfilament spacing. Biochemistry 36: 15035–15040.

Carden MJ, Trojanowski JQ, Schlaepfer WW, Lee VMY. 1987. Two-stage expression of neurofilament polypeptides during rat neurogenesis with early establishment of adult phosphorylation patterns. J Neurosci 7:3489–3504.

Chen JG, Nakata T, Zhang ZZ, Hirokawa N. 2000. The C-terminal tail domain of neurofilament protein-H (NF-H) forms the crossbridges and regulates neurofilament bundle formation. J Cell Sci 113:3861–3869.

Chin TK, Harding SE, Eagles PAM. 1989. Characterization of 2 proteolytically derived soluble polypeptides from the neurofilament triplet components nfm and nfh. Biochem J 264:53–60.

de Waegh SM, Lee VMY, Brady ST. 1992. Local modulation of neurofilament phosphorylation, axonal caliber, and slow axonal transport by myelinating schwann cells. Cell 68:451–463.

Doi M, Edwards SF. 1986. The theory of polymer dynamics. Oxford: Oxford University Press.

Galbraith JA, Reese TS, Schlief ML, Gallant PE. 1999. Slow transport of unpolymerized tubulin and polymerized neurofilament in the squid giant axon. Proc Natl Acad Sci USA 96:11589–11594.

Garde S, Khare R, Hummer G. 2000. Microscopic density fluctuations and solvation in polymeric fluids. J Chem Phys 112:1574–1578.

Geisler N, Weber K. 1981. Self-assembly in vitro of the 68,000 molecular-weight component of the mammalian neurofilament triplet proteins into intermediate-sized filaments. J Mol Biol 151:565–571.

Gou JP, Gotow T, Janmey PA, Leterrier JF. 1998. Regulation of neurofilament interactions in vitro by natural and synthetic polypeptides sharing lys-ser-pro sequences with the heavy neurofilament subunit NF-H: neurofilament crossbridging by antiparallel sidearm overlapping. Med Biol Eng Comput 36:371–387.

Hisanaga S, Hirokawa N. 1988. Structure of the peripheral domains of neurofilaments revealed by low-angle rotary shadowing. J Mol Biol 202:297–305.

Hsieh ST, Crawford TO, Griffin JW. 1994. Neurofilament distribution and organization in the myelinated axons of the peripheral nervous system. Brain Res 642:316–326.

Hummer G, Garde S, Garcia AE, Pohorille A, Pratt LR. 1996. An information theory model of hydrophobic interactions. Proc Natl Acad Sci U S A 93:8951–8955.

Leapman RD, Gallant PE, Reese TS, Andrews SB. 1997. Phosphorylation and subunit organization of axonal neurofilaments determined by scanning transmission electron microscopy. Proc Natl Acad Sci USA 94: 7820–7824.

Lee VMY, Otvos L, Carden MJ, Hollosi M, Dietzschold B, Lazzarini RA. 1988. Identification of the major multiphosphorylation site in mammalian neurofilaments. Proc Natl Acad Sci USA 85:1998–2002.

Leterrier JF, Kas J, Hartwig J, Vegners R, Janmey PA. 1996. Mechanical effects of neurofilament cross-bridges—modulation by phosphorylation, lipids, and interactions with F-actin. J Biol Chem 271:15687–15694.

Leung CL, Liem RKH. 1996. Characterization of interactions between the neurofilament triplet proteins by the yeast two-hybrid system. J Biol Chem 271:14041–14044.

Leung CL, Sun DM, Liem RKH. 1999. The intermediate filament protein peripherin is the specific interaction partner of mouse BPAG1-n (dystonin) in neurons. J Cell Biol 144:435–446.

Leung CL, Zheng M, Prater SM, Liem RKH. 2001. The BPAG1 locus: Alternative splicing produces multiple isoforms with distinct cytoskeletal linker domains, including predominant isoforms in neurons and muscles. J Cell Biol 154:691–697.

Likos CN, Vaynberg KA, Lowen H, Wagner NJ. 2000. Colloidal stabilization by adsorbed gelatin. Langmuir 16:4100–4108.

Lodge TP, Muthukumar M. 1996. Physical chemistry of polymers: Entropy, interactions, and dynamics. J Phys Chem 100:13275–13292.

Luckham P. 1996. Recent advances in polymers at surfaces: The steric effect. Curr Opin Colloid Interface Sci 1:39–47.

Martin R, Door R, Ziegler A, Warchol W, Hahn J, Breitig D. 1999. Neurofilament phosphorylation and axon diameter in the squid giant fibre system. Neuroscience 88:327–336.

Nixon RA, Paskevich PA, Sihag RK, Thayer CY. 1994. Phosphorylation on carboxyl-terminus domains of neurofilament proteins in retinal ganglion-cell neurons in vivo—influences on regional neurofilament accumulation, interneurofilament spacing, and axon caliber. J Cell Biol 126:1031–1046.

Pearson LT, Chan SI, Lewis BA, Engelman DM. 1983. Pair distribution-functions of bacteriorhodopsin and rhodopsin in model bilayers. Biophys J 43:167–174.

Perelson AS. 1978. Spatial-distribution of surface-immunoglobulin on B lymphocytes—local ordering. Exp Cell Res 112:309–321.

Pincus P. 1991. Colloid stabilization with grafted polyelectrolytes. Macromolecules 24:2912–2919.

Price RL, Paggi P, Lasek RJ, Katz MJ. 1988. Neurofilaments are spaced randomly in the radial dimension of axons. J Neurocytol 17:55–62.

Price RL, Lasek RJ, Katz MJ. 1993. Neurofilaments assume a less random architecture at nodes and in other regions of axonal compression. Brain Res 607:125–133.

Romero P, Obradovic Z, Kissinger CR, Villafranca JE, Garner E, Guilliot S, Dunker AK. 1998. Thousands of proteins likely to have long disordered regions. Pacific Symp Biocomput 3:437–448.

Szleifer I, Carignano MA. 1996. Tethered polymer layers. Adv Chem Phys 94:165–260.

Terada S, Nakata T, Peterson AC, Hirokawa N. 1996. Visualization of slow axonal transport in vivo. Science 273:784–788.

Tirrell M, Levicky R. 1997. End-tethered chain molecules at liquid interfaces. Curr Opin Solid State Mat Sci 2:668–672.

Wang L, Brown A. 2001. Rapid intermittent movement of axonal neurofilaments observed by fluorescence photobleaching. Mol Biol Cell 12: 3257–3267.

Wang L, Ho CL, Sun DM, Liem RKH, Brown A. 2000. Rapid movement of axonal neurofilaments interrupted by prolonged pauses. Nat Cell Biol 2:137–141.

Willard M, Simon C. 1981. Antibody decoration of neurofilaments. J Cell Biol 89:198–205.

Xu ZS, Marszalek JR, Lee MK, Wong PC, Folmer J, Crawford TO, Hsieh ST, Griffin JW, Cleveland DW. 1996. Subunit composition of neurofilaments specifies axonal diameter. J Cell Biol 133:1061–1069.

Yabe JT, Chylinski T, Wang FS, Pimenta A, Kattar SD, Linsley MD, Chan WKH, Shea TB. 2001. Neurofilaments consist of distinct populations that can be distinguished by C-terminal phosphorylation, bundling, and axonal transport rate in growing axonal neurites. J Neurosci 21:2195–2205.

Yang Y, Dowling J, Yu QC, Kouklis P, Cleveland DW, Fuchs E. 1996. An essential cytoskeletal linker protein connecting actin microfilaments to intermediate filaments. Cell 86:655–665.

Yang Y, Bauer C, Strasser G, Wollman R, Julien JP, Fuchs E. 1999. Integrators of the cytoskeleton that stabilize microtubules. Cell 98:229–238.

Yin X, Crawford TO, Griffin JW, Tu PH, Lee VMY, Li CM, Roder J, Trapp BD. 1998. Myelin-associated glycoprotein is a myelin signal that modulates the caliber of myelinated axons. J Neurosci 18:1953–1962.

Zhao B, Brittain WJ. 2000. Polymer brushes: surface-immobilized macromolecules. Progr Polym Sci 25:677–710.

Zilman AG, Safran SA. 2001. Entropically driven attraction between telechelic brushes. Eur Phys J E4:467–473.